Review

Recent Developments in Photocathodes for Solar-Driven Hydrogen Peroxide Production

Ying Zhang [1], Wanjun Tang [1], Yuchen Cong [1], and Lei Wang [2,*]

[1] School of Integrated Circuits, Anhui University, Hefei 230601, China
[2] Collaborative Innovation Center of Chemistry for Energy Materials (iChEM), Key Laboratory of Precision and Intelligent Chemistry, Department of Polymer Science and Engineering, University of Science and Technology of China, Hefei 230026, China
* Correspondence: lwang@ustc.edu.cn

Received: 8 July 2025; Revised: 21 August 2025; Accepted: 27 August 2025; Published: 29 August 2025

Abstract: Solar-driven photoelectrochemical (PEC) oxygen reduction reaction (ORR) using a photocathode that relies only on oxygen and water offers a promising on-site approach for hydrogen peroxide (H_2O_2) production. This method provides a sustainable and low-carbon alternative to the energy-intensive anthraquinone process. Both inorganic semiconductors and organic conjugated polymers have been developed as effective photocathode materials for PEC ORR, each with distinct advantages. Inorganic semiconductors generally generate free charge carriers with high mobilities, which leads to improved photocurrent densities. In contrast, organic conjugated polymers exhibit tunable band structures and allow molecular-level incorporation of catalytic sites that favor selective two-electron ORR. This review presents a comprehensive overview of recent advancements in photocathode development for H_2O_2 generation, focusing on both inorganic semiconductors and organic conjugated polymer-based materials. We emphasize key design strategies, including band structure engineering and active site modulation, to improve charge transfer efficiency and enhance product selectivity. Finally, we discuss the major challenges that currently limit photocathode development and outline emerging opportunities for future innovation. By providing these perspectives, this review seeks to guide the rational design of sustainable H_2O_2 production systems and contribute to the broader advancement of efficient solar-to-chemical energy conversion.

Keywords: photoelectrochemical; hydrogen peroxide; oxygen reduction reaction; structure-property relationship; solar-to-chemical energy conversion

1. Introduction

Hydrogen peroxide (H_2O_2) is a versatile oxidant widely applied in medical disinfection, bleaching, and chemical synthesis [1,2]. Beyond these conventional uses, H_2O_2 has increasingly been recognized as a potential energy carrier, capable of delivering usable power in fuel cells and other energy conversion devices [3]. Currently, more than 95% of global H_2O_2 production relies on the anthraquinone process. This method involves the noble-metal-catalyzed (e.g., Pd) hydrogenation of an alkyl anthraquinone to its hydroquinone form, followed by auto-oxidation with oxygen (O_2) to regenerate the anthraquinone and yield H_2O_2 (Figure 1) [4]. However, the process depends heavily on aromatic organic solvents and precious-metal catalysts, and it not only incurs significant energy costs but also generates metal-contaminated wastewater [5,6]. These drawbacks conflict with the principles of green chemistry and have driven extensive efforts to develop cost-effective and environmentally friendly alternatives.

Solar-driven photoelectrochemical (PEC) oxygen reduction reaction (ORR) using a photocathode that consumes only sunlight, O_2, and water provides a compelling on-site strategy for H_2O_2 production (Figure 2a) [7–9]. Compared with standalone particulate photocatalysis, PEC systems benefit from an internal electric field that promotes charge transport, enhances charge separation, and reduces recombination losses [10,11]. Unlike integrated photovoltaic–electrocatalytic devices, which require both light harvesting and an external power source, PEC architectures can operate under bias-free conditions when photoelectrodes are carefully designed. This feature enhances both energy and economic efficiency [12–14]. For example, Wu et al. demonstrated that by engineering a Ru/$Sb_2(S,Se)_3$ photoanode in combination with a Pt/TiO_2/Sb_2S_3 photocathode, an unassisted PEC system

powered entirely by sunlight could be constructed to simultaneously generate H_2O_2 and H_2 [15]. As a result, this integrated system achieved an average PEC H_2O_2 production rate of 0.637 μmol cm^{-2} min^{-1} without any external bias. Through band structure engineering and interface design, PEC platforms enable precise control over the two-electron ORR pathway, thereby maximizing H_2O_2 selectivity while also facilitating mechanistic studies and catalyst optimization [16–20]. Their inherent scalability and modularity further underscore their potential for efficient solar-to-chemical energy conversion in decentralized applications (Figure 2b).

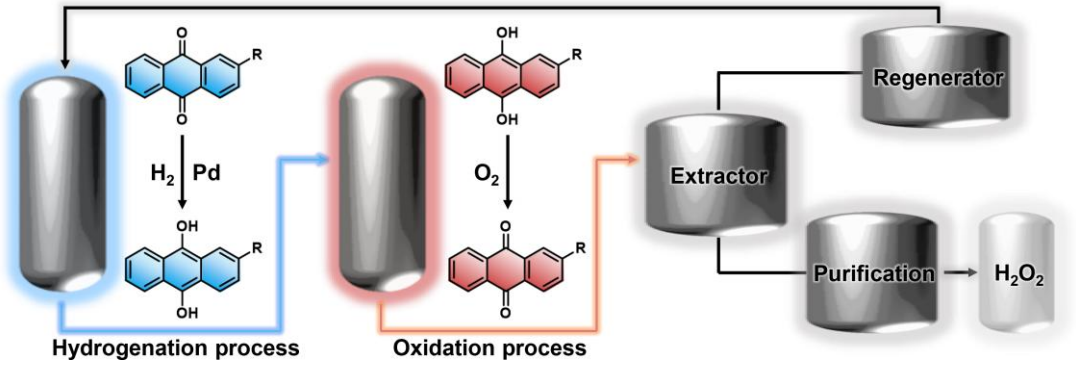

Figure 1. Schematic diagram of the industrial anthraquinone process for H_2O_2 production.

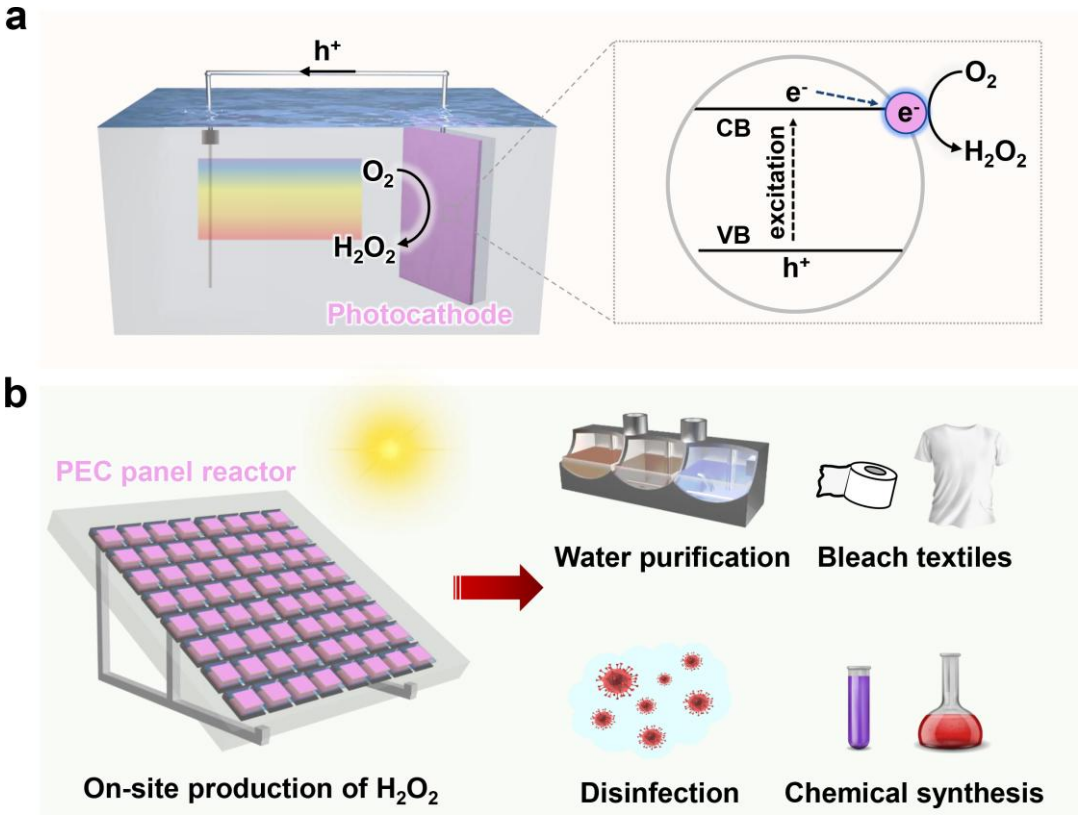

Figure 2. Schematic illustration of (**a**) the ORR process using a photocathode for solar-driven H_2O_2 production, where CB and VB represent the conduction and valence bands of the semiconductor, respectively; and (**b**) PEC panel reactor based on photocathodes for in situ H_2O_2 synthesis under real sunlight irradiation, along with its potential applications.

Over the past decade, a wide range of photocathode materials, including inorganic semiconductors [21–25] and organic conjugated polymers [26–34], have been developed (Table 1). Key approaches such as doping engineering, active-site modification, and heterojunction construction have been employed to improve charge separation and enhance product selectivity. These strategies have raised H_2O_2 production rates from the initial μmol h^{-1} range to the mmol h^{-1} level, while pushing faradaic efficiencies (FE) close to the theoretical maximum of 100%. Collectively, these advances demonstrate that PEC ORR represents an effective and scalable solar-driven pathway for H_2O_2 production.

Table 1. Summary of representative photocathodes for PEC ORR toward H_2O_2 production.

Classification	Photocathode materials	Light conditions	Applied bias voltage and solution pH	FE (%)	Photocurrent (μA cm^{-2})	H_2O_2 yield	Ref.
Inorganic semiconductors	Ca-$BiVO_4$/Pt/Ag	100 mW·cm^{-2}, AM 1.5G	0.8 V *vs.* RHE, pH = 3	46	110	/	[21]
	Ag-deposited Na-doped $BiFeO_3$	100 mW·cm^{-2}, AM 1.5G	0.8 V *vs.* RHE, pH = 7	40.1	~100	/	[22]
	Cu_3BiS_3/CdS/TiO_2/MoO_x/Mo	100 mW·cm^{-2}, AM 1.5G	0.35 V *vs.* RHE, pH = 12	97	4700	/	[23]
	p-BVO/SnO_2/NiNC	100 mW·cm^{-2}, AM 1.5G	0.4 V *vs.* RHE, pH = 6	76.1	150	338.84 μmol h^{-1} L^{-1}	[24]
	$CuBi_2O_4$/$PtSe_2$	laser (430 nm, 10 mW) with 0.2 mm^2	0.5 V *vs.* RHE, pH = 8.2	35	590	956 μmol h^{-1} L^{-1}	[25]
Organic conjugated polymers	EPI	60 mW·cm^{-2} from a halogen bulb	0.26 V *vs.* RHE, pH = 1	96	12~15	4.06 mg (H_2O_2) $g_{photocat}^{-1}$ h^{-1}	[26]
	pTTh	100 mW·cm^{-2}, AM 1.5G	0.6 V *vs.* RHE, pH = 12.9	~98	1700	10000 μmol h^{-1} L^{-1}	[27]
	pTTh	300 mW cm^{-2}, Xe lamp	0.6 V *vs.* RHE, pH = 13	~100	1200	/	[28]
	PPT	1.0 Sun	0.91 V *vs.* RHE, pH = 12	96	75	14 000 mg (H_2O_2) $g_{photocat}^{-1}$ h^{-1}	[29]
	pTh-BTD	100 mW·cm^{-2}, 1 sun	0.25 V *vs.* RHE, pH = 1	90	300~400	/	[30]
	NiO_x-TiO_2-PCN	420 nm LED	0.25 V *vs.* RHE, pH = 7	/	20	/	[31]
	rr-P3HT	1.0 Sun	0.71 V *vs.* RHE, pH=12	95	20	3900 mg (H_2O_2) $g_{photocat}^{-1}$ h^{-1}	[32]
	H_2Pc/PTCDI/Au/cat	100 mW·cm^{-2}	0.31 V *vs.* RHE, pH = 2	60~80	800	/	[33]
	CPF-CzAD	100 mW·cm^{-2}, AM 1.5G	0.7 V *vs.* RHE, pH = 8.2	95.5	1800	550 μmol h^{-1} L^{-1}	[34]

Despite significant breakthroughs, a comprehensive and systematic review of photocathode design strategies for solar-driven H_2O_2 production is still lacking. To address this gap, we provide an in-depth overview of recent progress in photocathode materials and architectures for H_2O_2 generation. We begin by outlining the fundamental mechanisms that govern PEC ORR at photocathodes. We then summarize the development of representative photocathodes, including inorganic semiconductors and organic conjugated polymers, with particular attention to design principles such as band structure engineering, surface active-site modulation, and heterojunction formation, all of which have been applied to improve reaction selectivity and overall performance. This review seeks to offer a coherent and comprehensive reference that can guide future research and accelerate the development of efficient photocathodes for solar-driven H_2O_2 synthesis.

2. Basic Principles for Solar-Driven H_2O_2 Production at the Photocathode

Solar-driven H_2O_2 production at a photocathode involves three fundamental steps: photoexcitation, charge separation and migration, and surface redox reactions (Figure 3a). When photons with energies exceeding the bandgap (E_g) are absorbed, electrons are excited from the valence band (VB) to the conduction band (CB), leaving holes in the VB. These holes are subsequently transferred to the counter electrode through the external circuit, while the photogenerated electrons in the CB migrate toward the photocathode-electrolyte interface to drive the ORR. To optimize charge separation and directional transport during the PEC process, built-in electric fields created by structures such as p-n junctions, Schottky contacts, or van der Waals heterojunctions are often integrated into photocathode designs. These internal fields promote efficient electron transfer to the semiconductor–electrolyte interface and thereby enhance the overall efficiency of H_2O_2 production.

H_2O_2 production at the photocathode-electrolyte interface proceeds through several competing ORR pathways (Figure 3b) [35]. In the direct two-electron pathway (Pathway I), molecular O_2 is reduced directly to H_2O_2 with a thermodynamic driving force defined by its standard potential (E = +0.68 V vs. NHE at pH = 0). This route is thermodynamically favorable but often suffers from sluggish kinetics. In the stepwise one-electron pathway (Pathway II), O_2 is first reduced to superoxide radicals ($\bullet O_2^-$; E = −0.33 V vs. NHE at pH = 0), which then undergo proton-coupled electron transfer to form H_2O_2. This pathway benefits from lower kinetic barriers due to single-electron intermediates, yet it can also trigger undesirable radical side reactions. Meanwhile, the two-electron hydrogen-evolution reaction (Pathway III) and the four-electron reduction of O_2 to water (Pathway IV) compete strongly, diverting electrons from H_2O_2 production and reducing selectivity.

The coexistence of multiple pathways at the photocathode-electrolyte interface requires carefully engineered photocathodes that direct electrons toward H_2O_2 formation by balancing kinetic accessibility with thermodynamic

driving force. First, the band structure of the photocathode must provide sufficient driving force for the two-electron ORR. Second, bulk and interfacial charge recombination must be minimized to ensure efficient charge separation. Third, active sites on the photocathode surface should be designed to stabilize key intermediates and lower activation barriers along the preferred two-electron ORR pathway. These requirements are essential for achieving high selectivity and overall efficiency in H_2O_2 production.

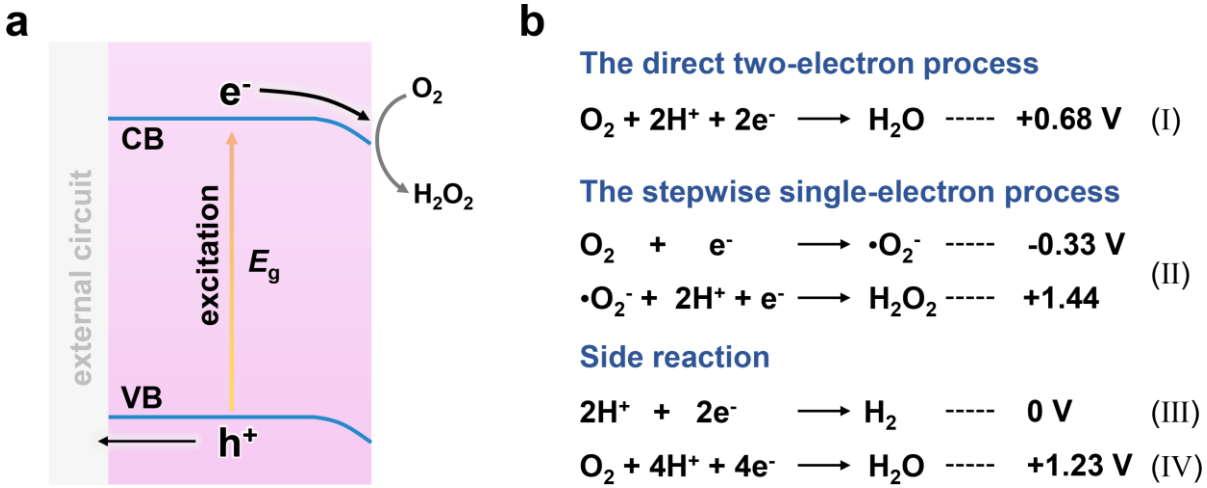

Figure 3. (**a**) Schematic illustration of the ORR processes at the photocathode for H_2O_2 production. (**b**) Surface chemical reactions on the photocathode, along with their corresponding potentials and associated charge transfer numbers.

Building on the above principles, the performance of photocathodes for H_2O_2 synthesis is determined by several interconnected factors, including band structures, charge separation, and surface-active sites. Broad light absorption combined with proper band alignment is essential for capturing photon energy across a wide spectral range to drive the ORR. Meanwhile, efficient charge separation and rapid charge transport are critical to reducing bulk and surface recombination losses, thereby improving H_2O_2 generation efficiency. A key bottleneck, however, lies in achieving selective two-electron ORR for H_2O_2 production, since competing four-electron ORR and single-electron O_2 reduction pathways can significantly lower selectivity. To address this challenge, photocathodes must be designed with precisely tailored catalytic sites that enable reliable two-electron ORR activity. Finally, long-term operational stability is indispensable for practical and scalable PEC systems. In summary, progress in photocathode design depends on materials that combine appropriate band structures, finely tuned active sites, and robust stability to ensure both selectivity and durability in PEC H_2O_2 synthesis.

3. Inorganic Semiconductors Photocathodes for H_2O_2 Production

Inorganic semiconductors such as metal oxides and sulfides are typically synthesized through sputtering, chemical vapor deposition, or physical vapor deposition [36–38]. Their inherent dopability and versatile fabrication methods allow precise control of both crystal structure and electronic properties, making them attractive candidates for PEC applications [39]. However, their ability to facilitate the two-electron ORR for H_2O_2 production remains underexplored. This limitation arises mainly from the scarcity of surface-active sites that can drive the kinetically demanding ORR, as well as intrinsically sluggish charge-transfer kinetics [40]. Recent research has therefore focused on strategically modifying both bulk and interfacial properties to address these issues.

One effective strategy is to engineer the surface-active sites of the photocathode to promote the two-electron ORR pathway. For example, Choi and co-workers transformed conventional n-type $BiVO_4$ into a p-type monoclinic-scheelite phase by doping it with Ca^{2+} under oxygen-rich conditions (denoted Ca-$BiVO_4$) (Figure 4a) [21]. Density-functional theory calculations revealed that the Ca^{2+} dopant introduces a shallow acceptor level about 30 meV above the hole polaron band, which facilitates hole formation at room temperature and significantly enhances p-type conductivity (Figure 4b). As shown in Figure 4c, the current density-potential (*J-V*) curves indicate that Ca-$BiVO_4$ exhibits a cathodic photocurrent onset near 1.1 V vs. RHE, which is more positive than that of typical p-type Cu_2O. However, in acidic media Ca-$BiVO_4$ alone produces almost no H_2O_2 due to the lack of adequate active sites. To overcome this limitation, the authors sequentially performed photo-electrodeposition of Pt followed by Ag nanoparticles (Figure 4d). The Pt layer improved electron extraction, while Ag selectively catalyzed the two-electron ORR pathway, leading to a 46% FE for H_2O_2 production. Building on this concept, the

same group later showed that Ag deposited on Na-doped $BiFeO_3$ could also drive the two-electron ORR, achieving a 40.1% FE at 0.8 V vs. RHE [41]. These studies illustrate that systematic surface-site engineering can substantially enhance solar-driven H_2O_2 production at photocathodes via the ORR.

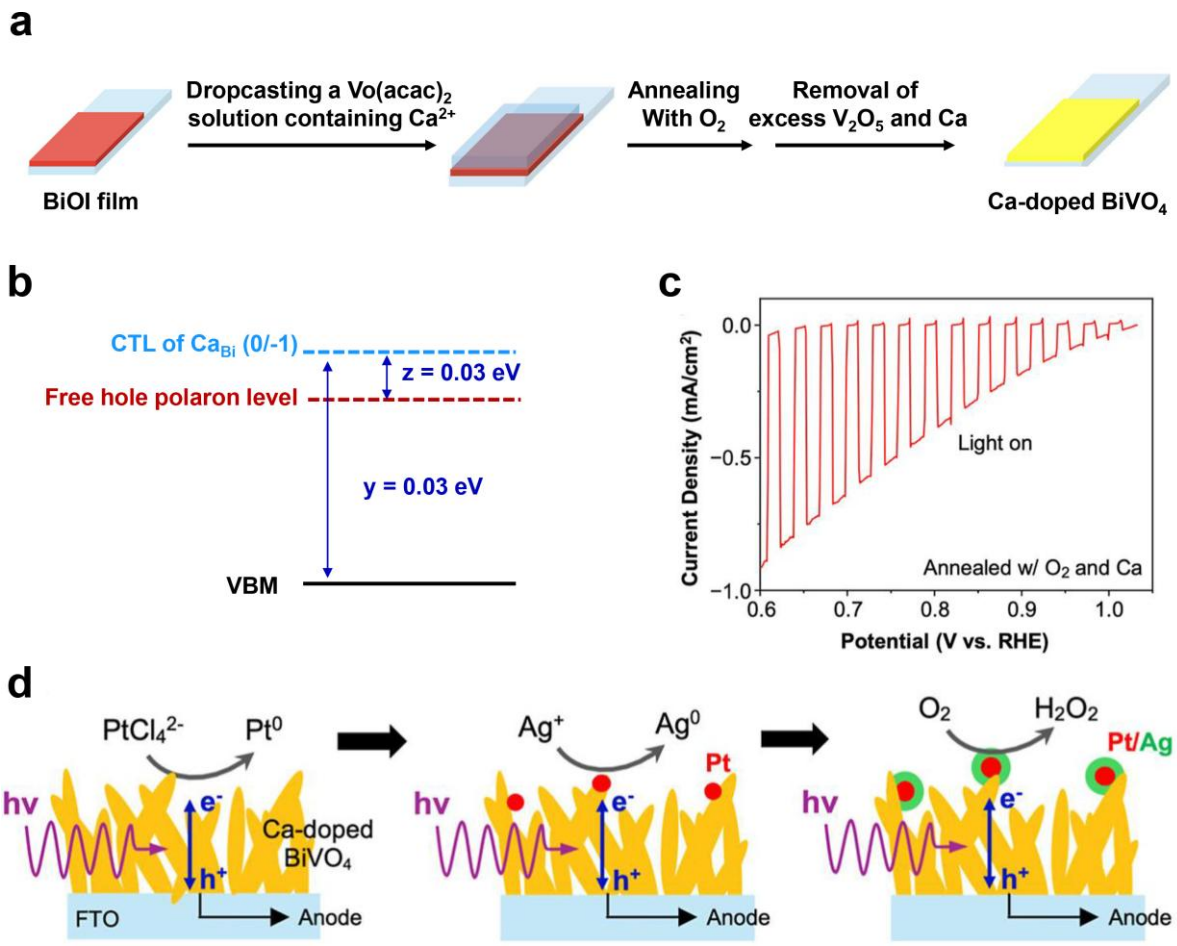

Figure 4. (**a**) Schematic representation of the Ca-$BiVO_4$ synthesis procedure. (**b**) Charge-state transition level (CTL) of Ca_{Bi} (0/−1) relative to the free-hole polaron level and the valence-band maximum (VBM). (**c**) *J-V* curves of Ca-$BiVO_4$ photocathodes under chopped AM 1.5 G illumination. (**d**) Schematic illustration of Pt/Ag photoelectrodeposition on Ca-$BiVO_4$ photocathodes and subsequent PEC H_2O_2 production. Reproduced with permission from Ref. [21]. Copyright 2025, American Chemical Society.

Beyond surface catalysis, minimizing charge recombination is also critical. Constructing heterojunctions to further enhance charge separation has therefore emerged as a promising strategy. For example, Moon et al. developed a Cu_3BiS_3-based photocathode by incorporating a Mo-anchored MoO_x layer through heterojunction design combined with cocatalyst integration [23]. In this architecture, MoO_x was first hydrothermally deposited onto the FTO/Au/Cu_3BiS_3/CdS/TiO_2 substrate, followed by sputtering a thin Mo catalyst layer on top of the MoO_x support (Figure 5a). As shown in Figure 5b, the incorporation of MoO_x and Mo generates a graded band structure that broadens light absorption and enhances carrier transport, thereby suppressing interfacial recombination losses. As a result, the Cu_3BiS_3/CdS/TiO_2/MoO_x/Mo photocathode achieved a high photocurrent density of 6.5 mA cm^{-2} at 0.2 V vs. RHE, which is significantly higher than that of Cu_3BiS_3/CdS/TiO_2 (~2.0 mA cm^{-2}) and Cu_3BiS_3/CdS/TiO_2/Mo (~3.8 mA cm^{-2}) (Figure 5c). Furthermore, in situ Raman spectroscopy revealed that MoO_x surface sites play a pivotal role in directing the ORR pathway. As shown in Figure 5d, compared with the bare Cu_3BiS_3 photocathode, peroxide intermediates exhibited stronger binding to dual Mo sites, which promoted the direct two-electron ORR toward H_2O_2 formation. Consequently, the Cu_3BiS_3/CdS/TiO_2/MoO_x/Mo photocathode achieved a Faradaic efficiency exceeding 97%.

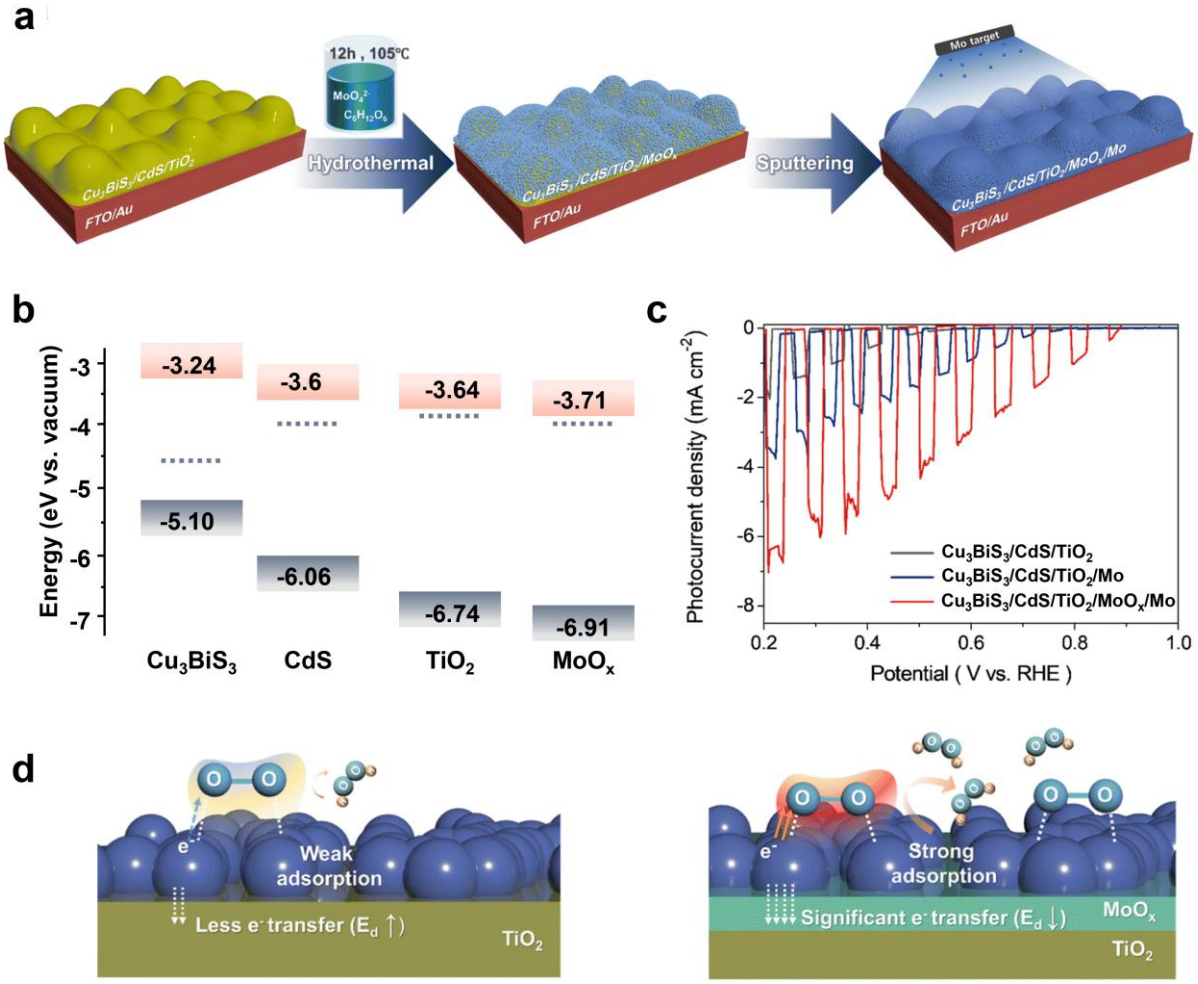

Figure 5. (**a**) Schematic illustration of MoO_x/Mo deposition onto the FTO/Au/Cu_3BiS_3/CdS/TiO_2 photocathode. (**b**) Simplified energy band diagram of the Cu_3BiS_3/CdS/TiO_2/MoO_x system. (**c**) *J*-*V* curves of various photocathodes. (**d**) Schematic of peroxide species adsorption on the photocathode surface during ORR. Reproduced with permission from Ref. [23]. Copyright 2024, Royal Society of Chemistry.

Another advancement was reported by Hou et al., who employed a stepwise fabrication strategy to construct a p-BVO/SnO_2/NiNC photocathode (Figure 6a) [24]. As shown in Figure 6b, compared with bare p-BVO, the favorable band alignment between SnO_2 and p-BVO facilitated rapid electron transfer from p-BVO to SnO_2, which improved carrier mobility and reduced bulk recombination. To further enhance selectivity toward the two-electron ORR pathway, a NiNC cocatalyst (Ni-doped, nitrogen-rich carbon) was integrated. LSV measurements showed that the p-BVO/SnO_2/NiNC photocathode delivered a much higher photocurrent density than both p-BVO and p-BVO/NiNC electrodes, highlighting the critical role of heterostructure design in promoting charge separation (Figure 6c). The p-BVO/SnO_2/NiNC photocathode achieved an H_2O_2 production rate of 65.46 μmol L^{-1} h^{-1} with a Faradaic efficiency of 76.12% (Figure 6d), far exceeding those of standalone p-BVO (8.87 μmol L^{-1} h^{-1}) and p-BVO/SnO_2 (9.32 μmol L^{-1} h^{-1}). Collectively, these results demonstrate that heterojunction construction effectively enhances charge separation in photocathodes, while surface cocatalysts improve ORR selectivity, thereby underscoring the potential of rationally engineered photocathode heterostructures to advance PEC H_2O_2 production.

Despite the significant potential demonstrated by heterojunction photocathodes in enhancing ORR performance, conventional fabrication methods such as chemical or physical epitaxial growth often require stringent preparation conditions. These methods are also prone to problems like lattice mismatch, which can lead to unfavorable charge recombination [41–43]. Such challenges increase interfacial carrier recombination and limit overall efficiency. To overcome these limitations, Feng et al. developed a $CuBi_2O_4$ (CBO)-based van der Waals (vdW) heterojunction photocathode with an Au/CBO/$PtSe_2$ architecture [25]. In this design, the p-type CBO light absorber is strategically positioned between an Au layer, which acts as a hole collector, and a $PtSe_2$ layer, which functions as an electron extractor (Figure 7a). This configuration takes advantage of the unique properties of vdW heterojunctions to facilitate efficient charge separation and transport. As depicted in Figure 7b, the CBO/$PtSe_2$ interface exhibits downward band bending, creating an energy barrier that blocks hole transfer from CBO to $PtSe_2$

while promoting efficient electron extraction. Meanwhile, the Au/CBO interface forms an ohmic contact, ensuring low-resistance hole collection. These synergistic effects result in a significant improvement in photocurrent density for the CBO/$PtSe_2$ photocathode compared with bare CBO, as illustrated in Figure 7c. Quantitative analyses further revealed enhanced charge-transfer and injection efficiencies upon forming the CBO/$PtSe_2$ heterojunction, confirming both effective charge separation and improved kinetics at the photoanode/electrolyte interface (Figure 7d,e). Moreover, as shown in Figure 7f, the bare CBO photocathode delivered a FE of only 27%, whereas the $PtSe_2$-decorated counterpart reached a substantially higher FE of 35%, demonstrating the superior ORR activity facilitated by $PtSe_2$. This study underscores the precise charge modulation and minimized interfacial losses achieved by van der Waals heterojunctions in solar-driven H_2O_2 synthesis.

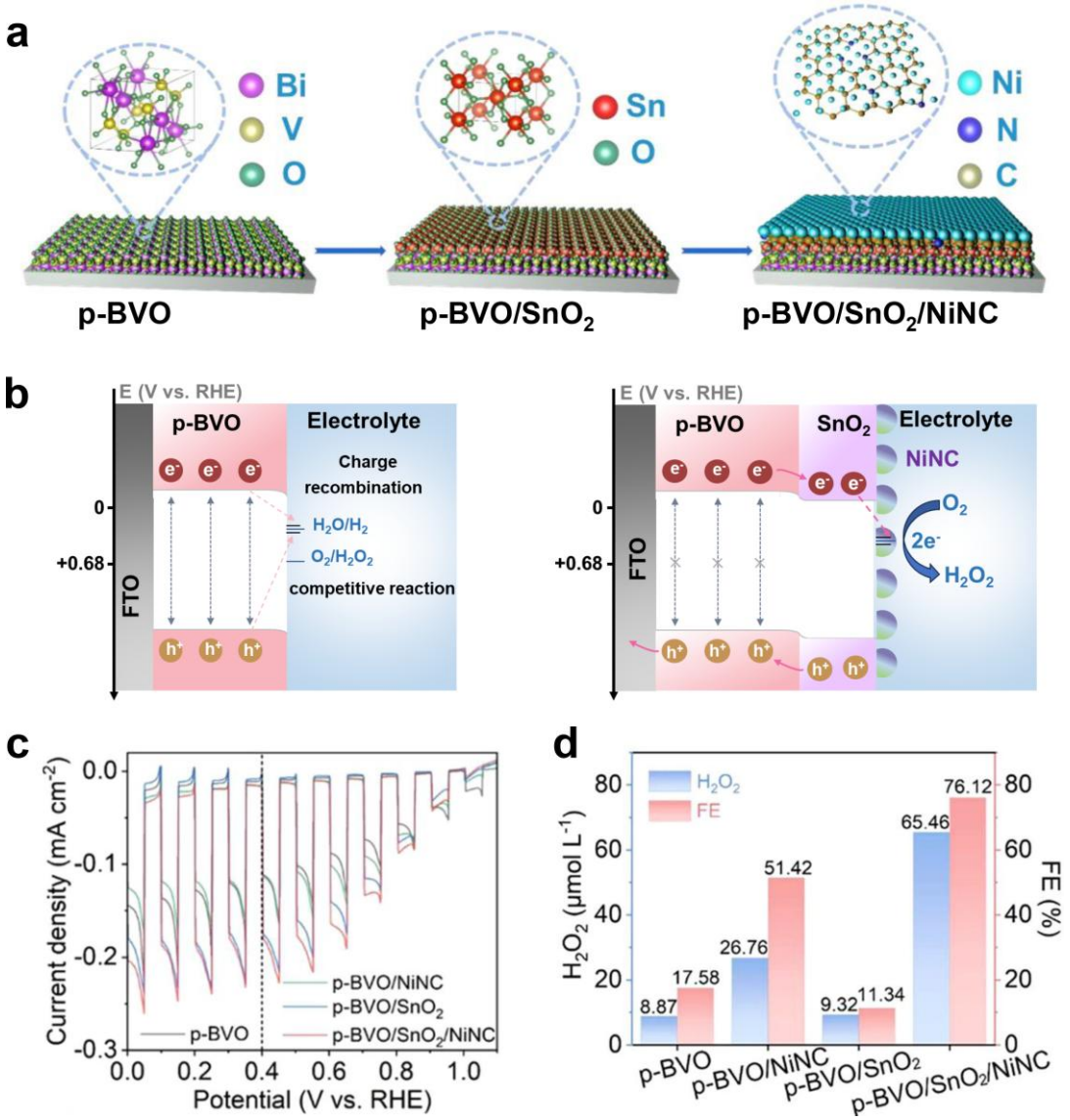

Figure 6. (**a**) Schematic of the p-BVO/SnO_2/NiNC photocathode fabrication process. (**b**) Charge-transfer pathways in p-BVO and p-BVO/SnO_2/NiNC photocathode. (**c**) *J-V* curves for different photocathodes. (**d**) H_2O_2 production rates and corresponding FE for different photocathodes. Reproduced with permission from Ref. [24]. Copyright 2024, American Chemical Society.

In addition to heterojunction construction for generating built-in electric fields and enhancing charge separation during PEC ORR toward H_2O_2 production, an alternative strategy combines thermoelectric and photoelectric effects. This approach harnesses the photothermal effect to produce internal electric fields that further optimize carrier dynamics. For instance, Zhang et al. designed a composite photocathode composed of $LaNiO_3$/$BiFeO_3$, where a p-type $BiFeO_3$ light-absorbing layer is deposited on a thermoelectric $LaNiO_3$ underlayer [44]. The $LaNiO_3$ absorbs near-infrared photons and converts them into heat, creating a temperature gradient that induces a thermoelectric voltage. This additional driving force spatially separates photogenerated electrons and holes, which reduces bulk recombination.

Together, these studies show that integrating surface cocatalysts, heterojunctions, and band engineering into inorganic photocathodes provides a powerful platform for solar-driven ORR to H_2O_2. Nevertheless, challenges remain. Cocatalysts often face limited long-term stability under acidic and oxidative conditions, and lattice mismatches during epitaxial heterojunction growth can create interfacial defects. Future efforts should therefore focus on atomic-level interface control to minimize recombination centers and on the development of robust, hierarchical architectures to improve durability. Moreover, combining in situ or operando characterization with high-throughput computational screening will be essential to uncover structure-activity relationships and guide the rational design of high-performance inorganic photocathodes for H_2O_2 production.

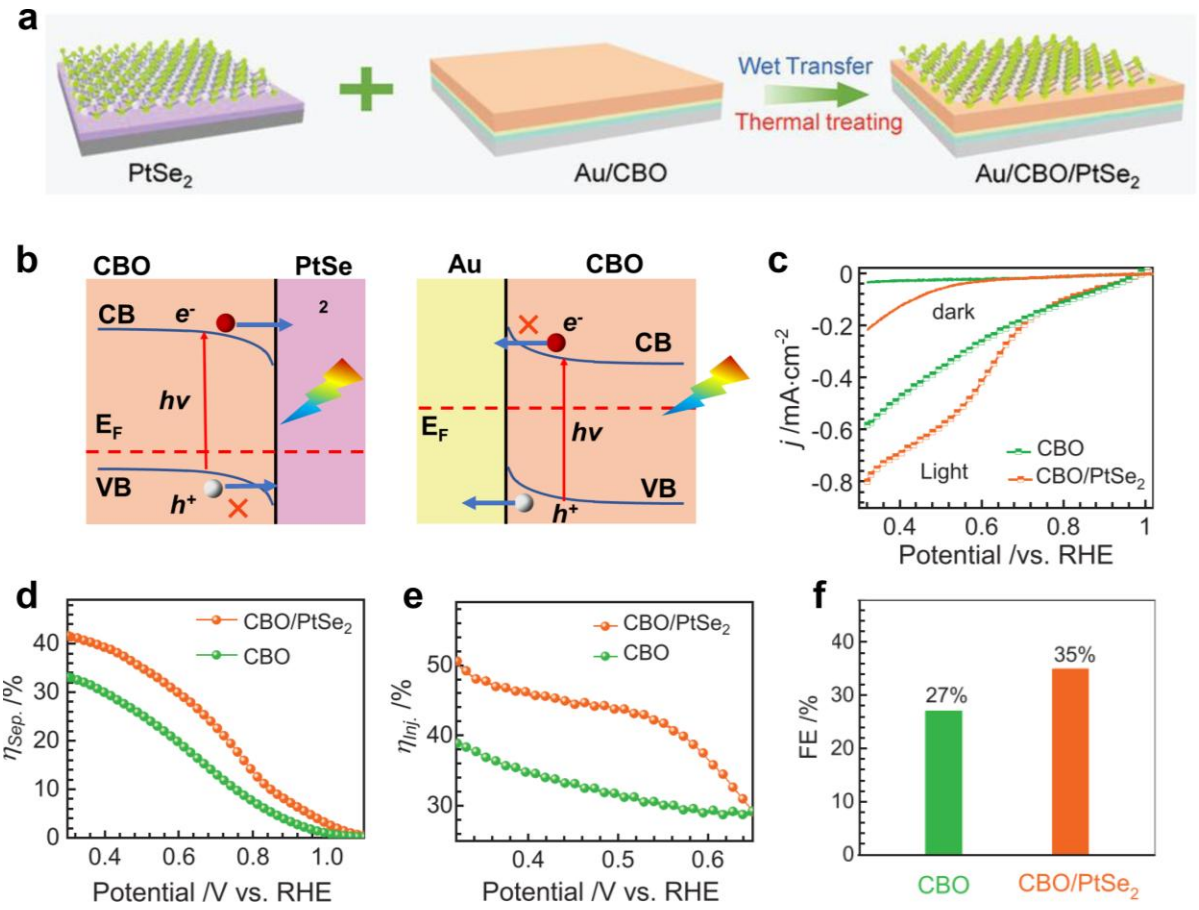

Figure 7. (**a**) Schematic illustration of the fabrication process of Au/CBO/$PtSe_2$ photocathodes. (**b**) Band alignments and charge carriers transport at CBO/$PtSe_2$ and Au/CBO interface. (**c**) *J-V* curves of different photocathodes. (**d**) The charge separation efficiency and (**e**) charge injection efficiency of different photocathodes. (**f**) FE of different photocathodes for the ORR towards H_2O_2 production. Reproduced with permission from Ref. [25]. Copyright 2023, John Wiley and Sons.

4. Organic Conjugated Polymer Photocathodes for H_2O_2 Production

As alternatives to inorganic semiconductors, organic conjugated polymer photocathodes have rapidly emerged as versatile platforms for H_2O_2 production because of their highly tunable chemical backbones, adjustable electronic structures, and the ability to precisely engineer surface-active sites [45–48]. Extensive studies have shown that rational modulation of surface reaction pathways in polymer photocathodes can enhance catalytic efficiency and product selectivity [49–51]. In addition, polymer photocathodes are compatible with scalable and cost-effective fabrication methods such as spin coating, dip coating, thermal vapor deposition, electrochemical polymerization, and solvothermal synthesis, which facilitates large-scale production and practical deployment [52–55].

In 2016, Glowacki and co-workers reported the first organic semiconductor photocathode for ORR toward H_2O_2, achieving stable peroxide generation under illumination in an acidic electrolyte over several days [26]. Inspired by this pioneering work, researchers have since developed a variety of polymer materials, including polythiophene (pTTh), carbon nitride, and donor–acceptor-type polymers [27–31]. Among these, polythiophene and its derivatives have been the most extensively studied for selective two-electron ORR because of their tunable electronic properties and the simplicity and low cost of their electrochemical synthesis. For example, Li et al.

demonstrated a metal-free pTTh photocathode that achieved both high efficiency and selectivity in solar-driven H_2O_2 production [27]. In situ electrochemical polymerization on carbon paper produced a film with broad light absorption extending to 640 nm and a narrow bandgap of approximately 2.0 eV (Figure 8a). Band-structure alignment measurements confirmed its suitability for H_2O_2 generation (Figure 8b). The photocurrent density displayed a strong dependence on pH. At pH 12.9, the pTTh photocathode reached −1.7 mA cm^{-2} at 0.6 V vs. RHE and an onset potential of 1.15 V, markedly outperforming its performance in acidic electrolyte (Figure 8c). Rotating ring-disk electrode measurements showed nearly 100% H_2O_2 selectivity through the HO_2^- pathway at pH 12.9, compared with only ~50% in acidic media (Figure 8d). These findings clearly indicate that electrolyte pH plays a decisive role in determining the selectivity of the photoelectrochemical ORR toward H_2O_2. Since ORR is a proton-coupled electron transfer process, the balance between protons and hydroxide ions directly governs the reaction pathway. Under alkaline conditions, the formation of HO_2^- as the final product is both thermodynamically and kinetically favored, while the competing four-electron pathway leading to water is effectively suppressed. Density functional theory calculations further supported this conclusion, showing that the energy barrier for HO_2^- formation is much lower than that for OH^- formation, with the two-electron step proceeding more than 200 times faster (Figure 8e,f). In contrast, in acidic conditions, the reduced hydroxide concentration and altered reaction energetics favor the four-electron pathway, lowering H_2O_2 selectivity. Thus, the exceptional selectivity of pTTh arises from the combined effect of its intrinsic electronic structure and surface-active sites. These results highlight the transformative potential of rationally engineered polymer photocathode reaction pathways for optimizing both catalytic efficiency and product selectivity in H_2O_2 synthesis.

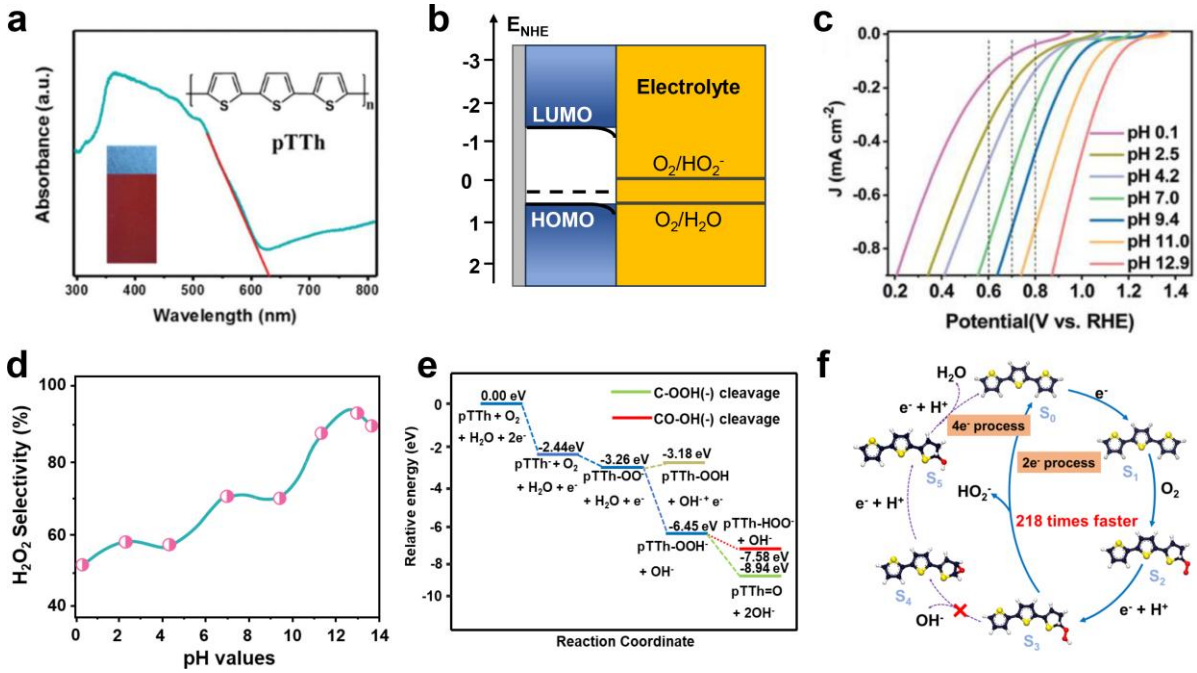

Figure 8. (**a**) UV-vis diffuse reflectance spectrum of pTTh; inset: molecular structure and photograph of the synthesized pTTh electrode. (**b**) Energy band alignment diagram of pTTh. (**c**) Linear sweep voltammograms of the pTTh electrode under illumination in O_2-saturated electrolytes at varying pH levels. (**d**) pH-dependent H_2O_2 selectivity of pTTh. (**e**) Calculated energy profiles for key ORR pathways on pTTh. (**f**) Proposed reaction cycles for H_2O_2 production at energetically favorable active sites on pTTh; S_o denotes the bare surface, and S_x (x = 1–5) represent intermediate-state structures. Reproduced with permission from Ref. [27]. Copyright 2020, Royal Society of Chemistry.

In contrast to inorganic photocathodes, which often rely on complex synthesis strategies such as doping or heterojunction engineering to achieve charge separation, polymer photocathodes can enhance charge separation and catalytic efficiency through rational molecular design. This strategy involves constructing conjugated polymers with alternating electron-rich donor units and electron-deficient acceptor units, which facilitates intramolecular charge transfer and reduces exciton binding energy [56,57]. Donor-acceptor (D-A) architectures thereby promote efficient separation of photogenerated carriers and directly improve photocatalytic performance. For instance, Oka et al. developed the conjugated copolymer poly[1,4-phenylene-alt-(2,2′-bisthiophene)-5,5′-diyl] (PPT), which incorporates alternating phenylene (acceptor) and thiophene (donor) units (Figure 9a) [29].

Incorporating electron-withdrawing phenylene groups into the thiophene backbone lowered the highest occupied molecular orbital (HOMO) level of the polymer by 0.3 eV compared with polyterthiophene, significantly enhancing photovoltage. The resulting PPT photocathode exhibited an exceptional onset potential of +1.53 V vs. RHE at pH 12 (Figure 9b). In situ Raman spectroscopy provided further mechanistic insight. The disappearance of the phenylene C–C stretching band at 1191 cm^{-1}, the emergence of an O–O stretching band at 881 cm^{-1}, and the decreased intensity of the phenylene C=C band at 1600 cm^{-1} confirmed that phenylene units, rather than thiophene moieties, serve as the active sites for selective H_2O_2 production through the two-electron ORR pathway (Figure 9c). This tailored electronic structure and interfacial activity enabled PPT to outperform polythiophene homopolymers, emphasizing the transformative role of molecular engineering in advancing polymer photocathode design.

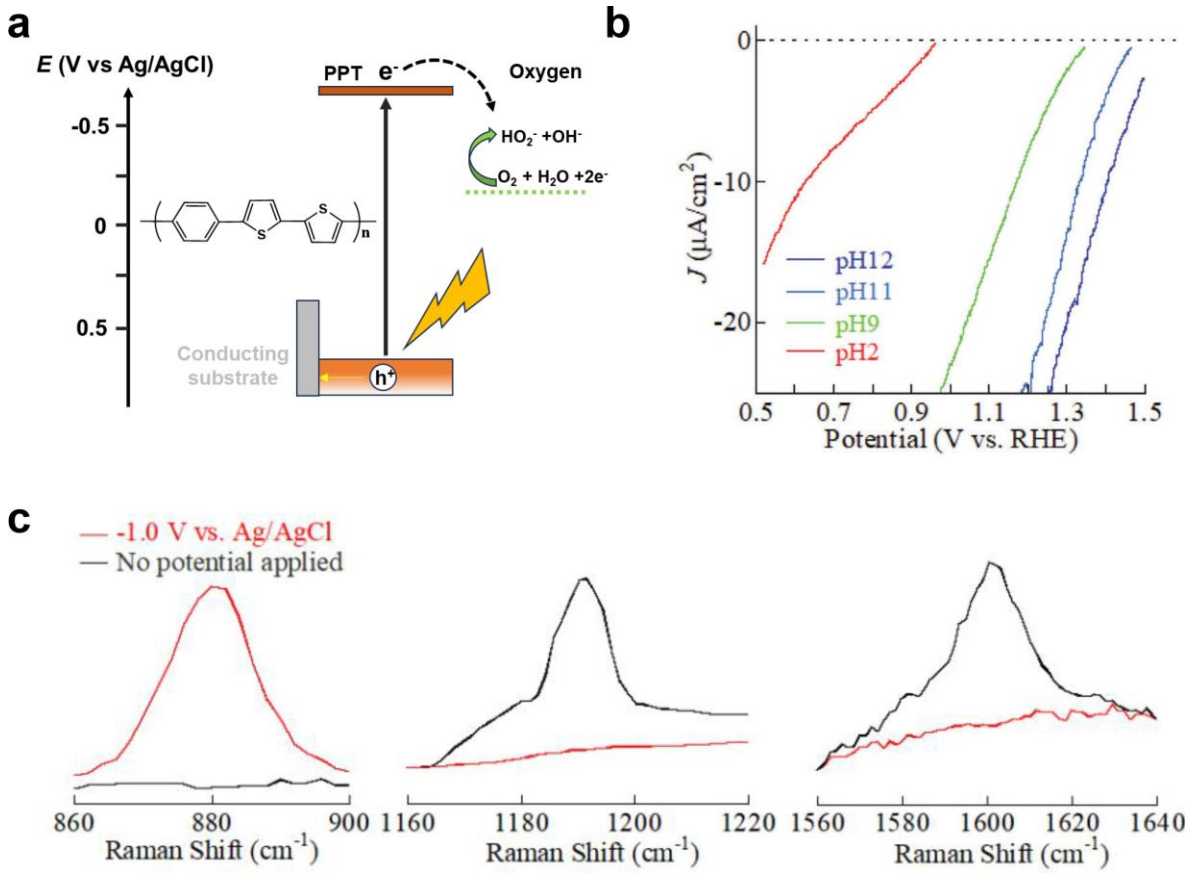

Figure 9. (**a**) Energy diagram of the PPT photocathode. (**b**) LSV of the PPT photocathode recorded under illumination in O_2-saturated electrolytes at varying pH levels. (**c**) In situ Raman spectra of the PPT photocathode during PEC ORR. Reproduced with permission from Ref. [29]. Copyright 2021, John Wiley and Sons.

Expanding on this strategy, Ganczarczyk et al. demonstrated that multi-D-A interactions in conjugated polymers can fine-tune electronic properties and optimize charge carrier distribution [30]. As shown in Figure 10a, their work employed benzothiadiazole (BTD), benzooxadiazole (BOD), and benzoselenadiazole (BSeD) acceptor cores functionalized with thiophene-based donor moieties in a D-A-D configuration. This design extended visible-light absorption into the red region, as in the case of pTh-BSeD, which absorbed at 623 nm, and simultaneously narrowed the optical bandgap. These improvements stemmed from the strong electron-withdrawing capacity of the acceptor units and the electron-donating ability of the thiophene derivatives. Electrochemical analyses further revealed HOMO and LUMO levels well aligned with the O_2/H_2O_2 redox potential (Figure 10b). For example, pTh-BTD exhibited a HOMO of −5.60 eV and a LUMO of −2.85 eV, enabling efficient hole extraction at the Au interface and electron transfer to O_2. Electropolymerized pTh-BTD films with porous microstructures delivered photocurrent densities as high as 300–400 μA/cm^2 under acidic conditions (Figure 10c). Moreover, pTh-BTD maintained a Faradaic efficiency above 90% for H_2O_2 production over 8 h of PEC operation, significantly outperforming conventional poly(3-hexylthiophene) systems (Figure 10d).

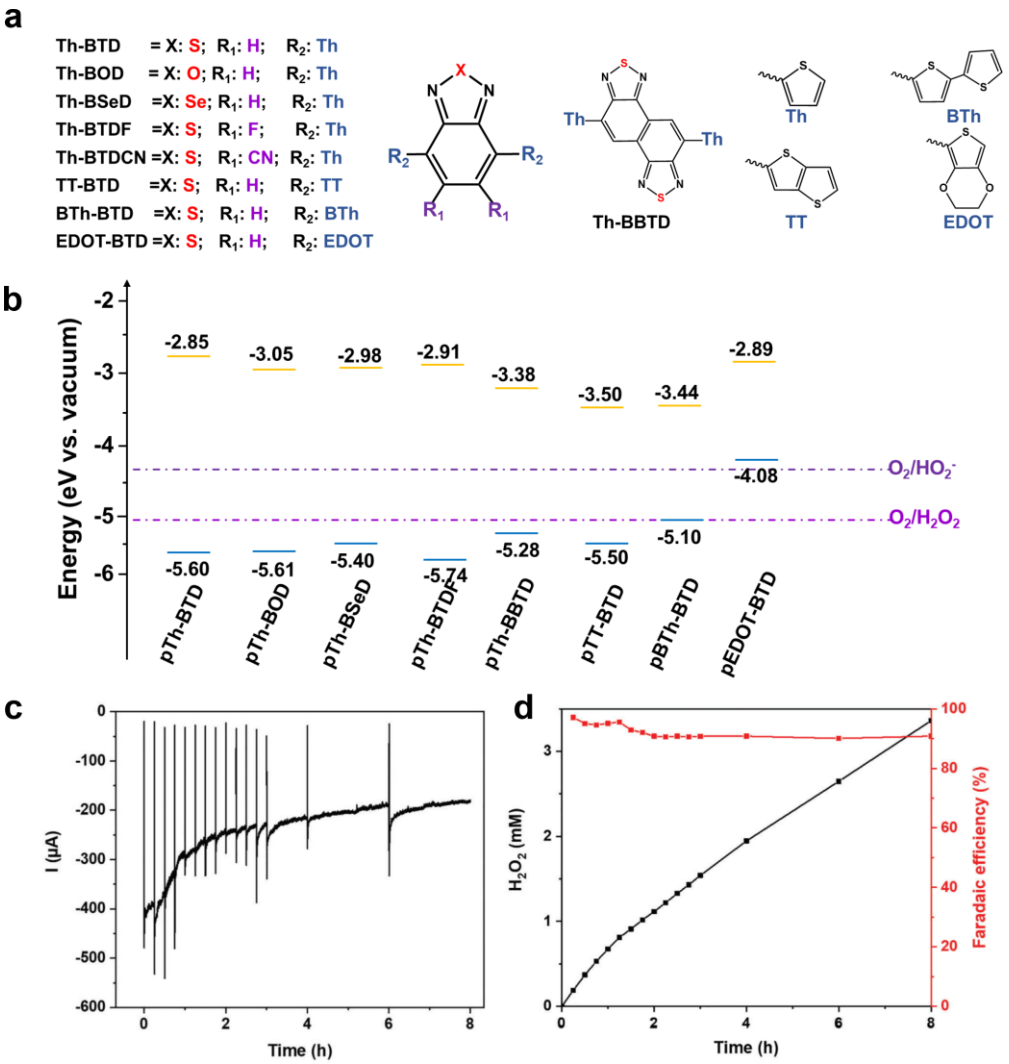

Figure 10. (**a**) Chemical structures of the investigated donor and acceptor groups. (**b**) Energy-level diagram showing the HOMO and LUMO of each polymer. (**c**) Chronoamperometric stability of the pTh-BTD photocathodes over 8 h of continuous irradiation. (**d**) Time-dependent faradaic efficiency (red trace) and corresponding H_2O_2 concentration in solution (black trace) for the pTh-BTD photocathodes. Reproduced with permission from Ref. [30]. Copyright 2023, John Wiley and Sons.

Overall, the intrinsic structural and electronic tunability of conjugated polymers provides powerful strategies for optimizing the ORR toward H_2O_2 production. A central aspect of this optimization is the molecular engineering of D-A architectures, which enhances visible-light harvesting and promotes efficient charge separation. Concurrently, rational design of surface-active sites is essential for steering reaction-pathway selectivity. However, improving overall performance, particularly photocurrent density, remains a major challenge because organic semiconductors typically exhibit high exciton binding energies (>100 meV), which hinder the generation of free carriers [58,59]. Polymers also suffer from low dielectric constants, usually between 3 and 5, which limit the spontaneous dissociation of photogenerated Frenkel excitons, namely coulombically bound electron-hole pairs [60]. Reducing exciton binding energy is therefore critical to improving H_2O_2 production in organic polymer semiconductors. For example, Wang et al. introduced ionic moieties into COF backbones to increase the dielectric constant and induce oriented polarization, thereby promoting exciton dissociation [61]. Compared with the neutral COF (DPTP), which had an exciton binding energy of 130 meV, the ionic COF (DBTP) exhibited a much higher dielectric constant and a substantially reduced exciton binding energy of 23 meV. As a result, DBTP achieved an H_2O_2 production rate of 10.01 mmol g^{-1} h^{-1}, compared with 1.47 mmol g^{-1} h^{-1} for DPTP, corresponding to an approximately 6.8-fold improvement. To overcome such intrinsic barriers in polymeric photocathodes, enhancing crystallinity to facilitate charge separation and carrier mobility is a promising strategy [62–64]. In addition, rationally designed multilayer heterojunctions or hybridization with inorganic semiconductors to establish built-in electric fields should further improve charge separation and overall PEC performance.

5. Conclusions and Perspective

Solar-driven H_2O_2 production from O_2 and water at a photocathode represents an attractive approach, as it relies solely on sunlight as the energy input. Over the past decade, two distinct classes of photocathode materials, inorganic semiconductors and conjugated polymers, have emerged as promising platforms. Strategies such as doping, cocatalyst incorporation, and heterojunction engineering have been employed to optimize band alignment, accelerate charge separation, and enrich surface active sites, thereby enhancing H_2O_2 generation rates. These advances demonstrate that rational photocathode design can simultaneously address the long-standing challenges of efficiency and stability that limit PEC ORR for H_2O_2 production.

Despite this progress, significant hurdles remain for solar-driven H_2O_2 production at photocathodes. Further refinement of material design and mechanistic understanding is required to achieve higher efficiencies [65–68]. Equally important, integrating advanced photocathodes into scalable and cost-effective PEC reactors poses a critical engineering challenge. High-quality inorganic photocathodes often rely on energy-intensive fabrication processes such as sputtering and chemical vapor deposition, yet still display insufficient long-term stability in aqueous media. Conversely, conjugated polymers generally suffer from large exciton binding energies, which promote rapid charge recombination and result in suboptimal PEC activity.

Recent studies have shown that hybrid photoelectrodes, created by combining rationally designed conjugated polymers with high-performance inorganic semiconductors, provide a promising pathway to advance PEC systems [69–71]. These hybrid architectures exhibit significantly enhanced photocurrent densities and improved operational stability. For example, coupling polycarbazole [34] or polytetrafluoroethylene [72] with $BiVO_4$ has been reported to synergistically promote charge separation and stabilize interfacial active sites, thereby improving both the efficiency and durability of H_2O_2 production. These results highlight that the rational design of polymer-inorganic hybrid photoelectrodes offers an effective means to overcome the efficiency-stability trade-off and accelerate progress in this field.

Beyond the development of efficient PEC systems, scaling from laboratory prototypes to practical large-scale H_2O_2 production reactors remains a formidable challenge [73,74]. While high efficiencies can be achieved on small electrodes, translating these performances to large-area devices faces obstacles such as non-uniform fabrication, limited interfacial charge transport, and mass transfer constraints [75,76]. Addressing these issues requires advanced device engineering, including the fabrication of uniform photoelectrode films through techniques such as inkjet printing or roll-to-roll coating, as well as the optimization of reactor designs to ensure effective photon utilization and electrolyte flow. Collectively, these strategies provide promising avenues toward scalable PEC systems.

PEC H_2O_2 production from abundant resources, namely O_2 and H_2O, holds great promise for sustainable chemical manufacturing and energy storage. Ongoing research in materials innovation and mechanistic understanding continues to advance photocathode technologies toward the performance and stability required for real-world applications. Ultimately, these developments may enable decentralized, carbon-neutral H_2O_2 production, contributing significantly to global clean-energy goals and a more sustainable future.

Funding: This work was supported by the National Natural Science Foundation of China (22209166), and the Fundamental Research Funds for the Central Universities (WK2060000077).

Conflicts of Interest: The author declares no conflict of interest.

References

1. Wang, Y.; Waterhouse, G.I.N.; Shang, L.; Zhang, T. Electrocatalytic Oxygen Reduction to Hydrogen Peroxide: From Homogeneous to Heterogeneous Electrocatalysis. *Adv. Energy Mater.* **2021**, *11*, 2003323.
2. Zhang, Y.; Xu, H. Backbone Engineering and Side Group Manipulation in Covalent Organic Frameworks for Overall Solar-Driven Hydrogen Peroxide Production. *Giant* **2024**, *20*, 100335.
3. Zhang, F.; Lv, X.; Wang, H.; Cai, J.; Wang, H.; Bi, S.; Wei, R.; Yang, C.; Zheng, G.; Han, Q. p-π Conjugated Covalent Organic Frameworks Expedite Molecular Triplet Excitons for H_2O_2 Production Coupled with Biomass Upgrading. *Adv. Mater.* **2025**, *37*, 2502220.
4. Chang, J.; Li, Q.; Shi, J.; Zhang, M.; Zhang, L.; Li, S.; Chen, Y.; Li, S.; Lan, Y. Oxidation-Reduction Molecular Junction Covalent Organic Frameworks for Full Reaction Photosynthesis of H_2O_2. *Angew. Chem. Int. Ed.* **2023**, *62*, e202218868.
5. Liu, Y.; Li, L.; Sang, Z.; Tao, H.; Ye, N.; Sun, C.; Sun, Z.; Luo, M.; Guo, S. Enhanced Hydrogen Peroxide Photosynthesis in Covalent Organic Frameworks Through Induced Asymmetric Electron Distribution. *Nat. Synth.* **2025**, *4*, 134–141.
6. Sun, Y.; Han, L.; Strasser, P. A Comparative Perspective of Electrochemical and Photochemical Approaches for Catalytic H_2O_2 Production. *Chem. Soc. Rev.* **2020**, *49*, 6605–6631.

7. Yang, C.; Xiang, Y.; Wang, W.; Cheng, B.; Yang, K.; Yu, J.; Cao, S. Enhancing Photocatalytic H_2O_2 Production of Donor−Acceptor Polymers by Modulation of Polymerization Modes. *Appl. Catal. B Environ. Energy* **2025**, *365*, 124856.
8. Cheng, J.; Wan, S.; Cao, S. Promoting Solar-Driven Hydrogen Peroxide Production Over Thiazole-Based Conjugated Polymers via Generating and Converting Singlet Oxygen. *Angew. Chem. Int. Ed.* **2023**, *62*, e202310476.
9. Freese, T.; Meijer, J.T.; Feringa, B.L.; Beil, S.B. An Organic Perspective on Photocatalytic Production of Hydrogen Peroxide. *Nat. Catal.* **2023**, *6*, 553–558.
10. Hou, H.; Zeng, X.; Zhang, X. Production of Hydrogen Peroxide by Photocatalytic Processes. *Angew. Chem. Int. Ed.* **2020**, *59*, 17356−17376.
11. Bu, Y.; Wang, Y.; Han, G.; Zhao, Y.; Ge, X.; Li, F.; Zhang, Z.; Zhong, Q.; Baek, J.-B. Carbon-Based Electrocatalysts for Efficient Hydrogen Peroxide Production. *Adv. Mater.* **2021**, *33*, 2103266.
12. Yu, F.; Zhou, Y.; Tan, H.; Li, Y.; Kang, Z. Versatile Photoelectrocatalysis Strategy Raising Up the Green Production of Hydrogen Peroxide. *Adv. Energy Mater.* **2023**, *13*, 2300119.
13. Ko, M.; Lim, J.S.; J.-Jang, W.; Joo, S.H. Bias-Free Photoelectrochemical H_2O_2 Production and its In-Situ Applications. *ACS. Est. Engg.* **2023**, *3*, 910–922.
14. Wu, H.; Tan, H.L.; Toe, C.Y.; Scott, J.; Wang, L.; Amal, R.; Ng, Y.H. Photocatalytic and Photoelectrochemical Systems: Similarities and Differences. *Adv. Mater.* **2020**, *32*, 1904717.
15. Wang, L.; Guo, F.; Ren, S.; Gao, R.T.; Wu, L. Unbiased Photoelectrochemical H_2O_2 Coupled to H_2 Production via Dual Sb_2S_3-Based Photoelectrodes with Ultralow Onset Potential. *Angew. Chem. Int. Ed.* **2024**, *63*, e202411305.
16. An, Y.; Lin, C.; Dong, C.; Wang, R.; Hao, J.; Miao, J.; Fan, X.; Min, Y.; Zhang, K. Scalable Photoelectrochemical Cell for Overall Solar Water Splitting into H_2 and H_2O_2. *ACS. Energy Lett.* **2024**, *9*, 1415–1422.
17. Lu, H.; Li, X.; Monny, S.A.; Wang, Z.; Wang, L. Photoelectrocatalytic Hydrogen Peroxide Production Based on Transition-Metal-Oxide Semiconductors. *Chin. J. Catal.* **2022**, *43*, 1204–1215.
18. Oka, K.; Winther-Jensen, B.; Nishide, H. Organic π-Conjugated Polymers as Photocathode Materials for Visible-Light-Enhanced Hydrogen and Hydrogen Peroxide Production from Water. *Adv. Energy Mater.* **2021**, *11*, 2003724.
19. Mehrotra, R.; Oh, D.; Jang, J.W. Unassisted Selective Solar Hydrogen Peroxide Production by an Oxidised Buckypaper-Integrated Perovskite Photocathode. *Nat. Commun.* **2021**, *12*, 6644.
20. Ge, Z.-Q.; Chu, C.; Wang, C.; Li, R.; Li, J.; Jiang, S.P. Recent Progress on Layered Double Hydroxides for Electrocatalytic Small Molecules Oxidation to Synthesize High-Value Chemicals and Degrade Pollutants. *Sci. Energy Environ.* **2024**, *1*, 10.
21. Seo, D.; Somjit, V.; Wi, D.H.; Galli, G.; Choi, K.-S. p-Type $BiVO_4$ for Solar O_2 Reduction to H_2O_2. *J. Am. Chem. Soc.* **2025**, *147*, 3261−3273.
22. Seo, D.; Grieder, A.; Radmilovic, A.; Alamudun, S.F.; Yun, X.; Ping, Y.; Choi, K.-S. Atomic Doping to Enhance The p-Type Behavior of $BiFeO_3$ Photoelectrodes for Solar H_2O_2 Production. *J. Mater. Chem. A* **2024**, *12*, 20437.
23. Moon, S.; Park, Y.S.; Lee, H.; Jeong, W.; Kwon, E.; Lee, J.; Yun, J.; Lee, S.; Kim, J.H.; Yu, S.; et al. Unassisted Photoelectrochemical Hydrogen Peroxide Production Over MoO_x-Supported Mo on A Cu_3BiS_3 Photocathode. *Energy Environ. Sci.* **2024**, *17*, 5588.
24. Shi, S.; Song, Y.; Jiao, Y.; Jin, D.; Li, Z.; Xie, H.; Gao, L.; Sun, L.; Hou, J. $BiVO_4$-Based Heterojunction Photocathode for High-Performance Photoelectrochemical Hydrogen Peroxide Production. *Nano Lett.* **2024**, *24*, 6051.
25. Zhang, Z.; Chen, X.; Hao, R.; Feng, Q.; Xie, E. Van Der Waals Heterojunction Modulated Charge Collection for H_2O_2 Production Photocathode. *Adv. Funct. Mater.* **2023**, *33*, 2303391.
26. Jakesova, M.; Apaydin, D.H.; Sytnyk, M.; Oppelt, K.; Heiss, W.; Sariciftci, N.S.; Glowacki, E.D. Hydrogen-Bonded Organic Semiconductors as Stable Photoelectrocatalysts for Efficient Hydrogen Peroxide Photosynthesis. *Adv. Funct. Mater.* **2016**, *26*, 5248–5254.
27. Fan, W.; Zhang, B.; Wang, X.; Ma, W.; Li, D.; Wang, Z.; Michel, D.; Shi, J.; Liao, S.; Li, C. Efficient Hydrogen Peroxide Synthesis by Metal-Free Polyterthiophene via Photoelectrocatalytic Dioxygen Reduction. *Energy Environ. Sci.* **2020**, *13*, 238–245.
28. Zhang, B.; Wang, S.; Fan, W.; Ma, W.; Liang, Z.; Shi, J.; Liao, S.; Li, C. Photoassisted Oxygen Reduction Reaction in H_2–O_2 Fuel Cells. *Angew. Chem. Int. Ed.* **2016**, *55*, 14748–14751.
29. Oka, K.; Nishide, H.; Winther-Jensen, B. Copolymer of Phenylene and Thiophene Toward a Visible-Light-Driven Photocatalytic Oxygen Reduction to Hydrogen Peroxide. *Adv. Sci.* **2021**, *8*, 2003077.
30. Ganczarczyk, R.; Rybakiewicz-Sekita, R.; Gryszel, M.; Drapała, J.; Zagorska, M.; Glowacki, E.D. Polymeric Benzothiadiazole, Benzooxadiazole, and Benzoselenadiazole Photocathodes for Photocatalytic Oxygen Reduction to Hydrogen Peroxide. *Adv. Mater. Interfaces* **2023**, *10*, 2300270.
31. Braun, H.; Mitoraj, D.; Kuncewicz, J.; Hellmann, A.; Elnagar, M.M.; Bansmann, J.; Kranz, C.; Jacob, T.; Macyk, W.; Beranek, R. Polymeric carbon nitride-based photocathodes for visible light-driven selective reduction of oxygen to hydrogen peroxide. *Appl. Catal. A Gen.* **2023**, *660*, 119173.

32. Oka, K.; Kamimori, K.; Winther-Jensen, B.; Nishide, H. Poly(3-alkylthiophene) Films as Solvent-Processable Photoelectrocatalysts for Efficient Oxygen Reduction to Hydrogen Peroxide. *Adv. Energy Sustain. Res.* **2021**, *2*, 2100103.
33. Gryszel, M.; Markov, A.; Vagin, M.; Glowacki, E.D. Organic Heterojunction Photocathodes for Optimized Photoelectrochemical Hydrogen Peroxide Production. *J. Mater. Chem. A* **2018**, *6*, 24709–24716.
34. Wang, L.; Wu, Y.; Mao, S.; Zhou, J.; Zhang, Y.; Zheng, X.; Wu, X.; Xu, H. Bias-Free Photoelectrochemical System for Scalable Solar-Driven Hydrogen Peroxide Production via Molecularly Engineered Conjugated Polycarbazole Frameworks. *Adv. Mater.* **2025**, e08326. https://doi.org/10.1002/adma.202508326.
35. Cheng, H.; Cheng, J.; Wang, L.; Xu, H. Reaction Pathways Toward Sustainable Photosynthesis of Hydrogen Peroxide by Polymer Photocatalysts. *Chem. Mater.* **2022**, *34*, 4259–4273.
36. Wu, B.; Wang, T.; Liu, B.; Li, H.; Wang, Y.; Wang, S.; Zhang, L.; Jiang, S.; Pei, C.; Gong, J. Stable Solar Water Splitting with Wettable Organic-Layer-Protected Silicon Photocathodes. *Nat. Commun.* **2022**, *13*, 4460.
37. Kenney, M.J.; Gong, M.; Li, Y.; Wu, J.Z.; Feng, J.; Lanza, M.; Dai, H. High-Performance Silicon Photoanodes Passivated with Ultrathin Nickel Films for Water Oxidation. *Science* **2013**, *342*, 836.
38. Chung, C.C.; Yeh, H.; Wu, P.H.; Lin, C.C.; Li, C.S.; Yeh, T.T.; Chou, Y.; Wei, C.Y.; Wen, C.Y.; Chou, Y.C.; et al. Atomic-Layer Controlled Interfacial Band Engineering at Two-Dimensional Layered $PtSe_2$/Si Heterojunctions for Efficient Photoelectrochemical Hydrogen Production. *ACS. Nano* **2021**, *15*, 4627–4635.
39. Vilanova, A.; Dias, P.; Lopes, T.; Mendes, A. The Route for Commercial Photoelectrochemical Water Splitting: A Review of Large-Area Devices and Key Upscaling Challenges. *Chem. Soc. Rev.* **2024**, *53*, 2388–2434.
40. Corby, S.; Rao, R.R.; Steier, L.; Durrant, J.R. The Kinetics of Metal Oxide Photoanodes from Charge Generation to Catalysis. *Nat. Rev. Mater.* **2021**, *6*, 1136–1155.
41. Wang, Z.; Wu, L.; Cheng, J.; Chen, H.; Luo, J. Gradient Surface Gallium-Doped Hematite Photoelectrode for Enhanced Photoelectrochemical Water Oxidation. *Nano Lett.* **2025**, *25*, 707–714.
42. Yan, Z.; Sun, H.; Chen, X.; Liu, H.; Zhao, Y.; Li, H.; Xie, W.; Cheng, F.; Chen, J. Anion Insertion Enhanced Electrodeposition of Robust Metal Hydroxide/Oxide Electrodes for Oxygen Evolution. *Nat. Commun.* **2018**, *9*, 2373.
43. Xu, J.; Che, H.; Tang, C.; Liu, B.; Ao, Y. Tandem Fields Facilitating Directional Carrier Migration in Van Der Waals Heterojunction for Efficient Overall Piezo-Synthesis of H_2O_2. *Adv. Mater.* **2024**, *36*, 2404539.
44. Tan, B.; Sun, M.; Liu, B.; Jiang, X.; Feng, Q.; Xie, E.; Xi, P.; Zhang, Z. Boosting Photocarrier Collection in Semiconductors by Synergizing Photothermoelectric and Photoelectric. *Nano Energy* **2023**, *107*, 108138.
45. Thangamuthu, M.; Ruan, Q.; Ohemeng, P.O.; Luo, B.; Jing, D.; Godin, R.; Tang, J. Polymer Photoelectrodes for Solar Fuel Production: Progress and Challenges. *Chem. Rev.* **2022**, *122*, 11778–11829.
46. Wang, L.; Xun, H. Two-Dimensional Conjugated Polymer Frameworks for Solar Fuel Generation from Water. *Prog. Polym. Sci.* **2023**, *145*, 101734.
47. Cheng, J.; Wu, Y.; Zhang, W.; Zhang, J.; Wang, L.; Zhou, M.; Fan, F.; Wu, X.; Xu, H. Fully Conjugated 2d Sp^2 Carbon-Linked Covalent Organic Frameworks for Photocatalytic Overall Water Splitting. *Adv. Mater.* **2024**, *36*, 2305313.
48. Chen, L.; Wang, L.; Wan, Y.; Zhang, Y.; Qi, Z.; Wu, X.; Xu, H. Acetylene and Diacetylene Functionalized Covalent Triazine Frameworks as Metal-Free Photocatalysts for Hydrogen Peroxide Production: A New Two-Electron Water Oxidation Pathway. *Adv. Mater.* **2020**, *32*, 1904433.
49. Zhang, P.; Li, L.; Zhao, J.; Wang, H.; Zhang, X.; Xie, Y. Elemental Doping Boosts Charge-Transfer Excitonic States in Polymeric Photocatalysts for Selective Oxidation Reaction. *Precis. Chem.* **2023**, *1*, 40–48.
50. Liao, Q.; Sun, Q.; Xu, H.; Wang, Y.; Xu, Y.; Li, Z.; Hu, J.; Wang, D.; Li, H.; Xi, K. Regulating Relative Nitrogen Locations of Diazine Functionalized Covalent Organic Frameworks for Overall H_2O_2 Photosynthesis. *Angew. Chem. Int. Ed.* **2023**, *62*, e202310556.
51. Luo, Y.; Zhang, B.; Liu, C.; Xia, D.; Ou, X.; Cai, Y.; Zhou, Y.; Jiang, J.; Han, B. Sulfone-Modified Covalent Organic Frameworks Enabling Efficient Photocatalytic Hydrogen Peroxide Generation via One-Step Two-Electron O_2 Reduction. *Angew. Chem. Int. Ed.* **2023**, *62*, e202305355.
52. Xu, W.; Meng, L.; Tian, W.; Li, S.; Cao, F.; Li, L. Polypyrrole Serving as Multifunctional Surface Modifier for Photoanode Enables Efficient Photoelectrochemical Water Oxidation. *Small* **2022**, *18*, e2105240.
53. Wang, Y.; Shi, H.; Cui, K.; Yu, J. Engineering Organic/Inorganic Hierarchical Photocathode for Efficient and Stable Quasi-Solid-State Photoelectrochemical Fuel Cells. *Appl. Catal. B* **2019**, *250*, 171–180.
54. Ng, C.H.; Winther-Jensen, O.; Ohlin, C.A.; Winther-Jensen, B. Exploration and Optimisation of Poly(2,2′-Bithiophene) as a Stable Photo-Electrocatalyst for Hydrogen Production. *J. Mater. Chem. A* **2015**, *3*, 11358–11366.
55. Sun, H.; Dong, C.; Liu, Q.; Yuan, Y.; Zhang, T.; Zhang, J.; Hou, Y.; Zhang, D.; Feng, X. Conjugated Acetylenic Polymers Grafted Cuprous Oxide as an Efficient Z-Scheme Heterojunction for Photoelectrochemical Water Reduction. *Adv. Mater.* **2020**, *32*, e2002486.
56. Cheng, H.; Lv, H.; Cheng, J.; Wang, L.; Wu, X.; Xu, H. Rational Design of Covalent Heptazine Frameworks with Spatially Separated Redox Centers for High-Efficiency Photocatalytic Hydrogen Peroxide Production. *Adv. Mater.* **2022**,

34, 2107480.

57. Xia, Y.; Zhang, W.; Yang, S.; Wang, L.; Yu, G. Research Progress in Donor−Acceptor Type Covalent Organic Frameworks. *Adv. Mater.* **2023**, *35*, 2301190.
58. Xu, B.; Yi, X.; Huang, T.Y.; Zheng, Z.; Zhang, J.; Salehi, A.; Coropceanu, V.; Ho, C.H.Y.; Marder, S.R.; Toney, M.F.; et al. Donor Conjugated Polymers with Polar Side Chain Groups: The Role of Dielectric Constant and Energetic Disorder on Photovoltaic Performance. *Adv. Funct. Mater.* **2018**, *28*, 1803418.
59. Mikhnenko, V.; Blom, P.W.M.; Nguyen, T.-Q. Exciton Diffusion in Organic Semiconductors. *Energy Environ. Sci.* **2015**, *8*, 1867–1888.
60. Wang, H.; Jin, S.; Zhang, X.; Xie, Y. Excitonic Effects in Polymeric Photocatalysts. *Angew. Chem. Int. Ed.* **2020**, *59*, 22828.
61. Li, G.; Fu, P.; Yue, Q.; Ma, F.; Zhao, X.; Dong, S.; Han, X.; Wang, J. Boosting Exciton Dissociation by Regulating Dielectric Constant in Covalent Organic Framework for Photocatalysis. *Chem Catal.* **2022**, *2*, 1734–1747.
62. Zhang, W.; Zhong, Z.; Wei, X.; Zhang, Y.; Ma, W.; Liu, D.; Han, X.; Dong, J.; Gong, W.; Dai, D.; et al. Single-Crystal Metal–Organic and Covalent Organic Framework Hybrids Enable Efficient Photoelectrochemical CO_2 Reduction to Ethanol. *J. Am. Chem. Soc.* **2025**, *147*, 17975–17984.
63. Yao, L.; Rodriguez-Camargo, A.; Xia, M.; Mucke, D.; Guntermann, R.; Liu, Y.; Grunenberg, L.; Jimenez-Solano, A.; Emmerling, S.T.; Duppel, V.; et al. Covalent Organic Framework Nanoplates Enable Solution-Processed Crystalline Nanofilms for Photoelectrochemical Hydrogen Evolution. *J. Am. Chem. Soc.* **2022**, *144*, 10291–10300.
64. Weng, W.; Guo, J. Chiral Covalent Organic Framework Films with Enhanced Photoelectrical Performances. *J. Am. Chem. Soc.* **2024**, *146*, 13201–13209.
65. Li, J.; Huang, Z.; Wang, C.; Tian, L.; Yang, X.; Zhou, R.; Ghazzal, N.M.; Liu, Z.-Q. Linkage Effect in the Bandgap-broken V_2O_5-$GdCrO_3$ Heterojunction by Carbon Allotropes for Boosting Photocatalytic H_2 Production. *Appl. Catal. B Environ.* **2024**, *340*, 123181.
66. Li, J.; Xiang, T.; Liu, X.; Ghazzal, M.N.; Z.-Liu, Q. Structure-Function Relationship of p-Block Bismuth for Selective Photocatalytic CO_2 Reduction. *Angew. Chem. Int. Ed.* **2024**, *63*, e202407287.
67. Li, J.; Wang, X.; Fang, H.; Guo, X.; Zhou, R.; Wang, C.; Li, J.; Ghazzal, M.N.; Rui, Z. Unraveling the Role of Surface and Interfacial Defects in Hydrogen Production to Construct an All-in-one Broken-gap Photocatalyst. *J. Mater. Chem. A* **2023**, *11*, 25639–25649.
68. Li, J.; Fang, H.; Wu, M.; Ma, C.; Lian, R.; Jiang, S.P.; Ghazzal, M.N.; Rui, Z. Selective Cocatalyst Decoration of Narrow-Bandgap Broken-Gap Heterojunction for Directional Charge Transfer and High Photocatalytic Properties. *Small* **2023**, *19*, 2300559.
69. Zhang, Y.; Lv, H.; Zhang, Z.; Wang, L.; Wu, X.; Xu, H. Stable Unbiased Photo-Electrochemical Overall Water Splitting Exceeding 3% Efficiency via Covalent Triazine Framework/Metal Oxide Hybrid Photoelectrodes. *Adv. Mater.* **2021**, *33*, e2008264.
70. Wang, L.; Lian, W.; Liu, B.; Lv, H.; Zhang, Y.; Wu, X.; Wang, T.; Gong, J.; Chen, T.; Xu, H. A Transparent, High-Performance, and Stable Sb_2S_3 Photoanode Enabled by Heterojunction Engineering with Conjugated Polycarbazole Frameworks for Unbiased Photoelectrochemical Overall Water Splitting Devices. *Adv. Mater.* **2022**, *34*, e2200723.
71. Yang, W.; Kwon, H.R.; Ji, S.G.; Kim, J.; Lee, S.A.; Lee, T.H.; Choi, S.; Cheon, W.S.; Kim, Y.; Park, J.; et al. Conjugated Polythiophene Frameworks as a Hole-Selective Layer on Ta_3N_5 Photoanode for High-Performance Solar Water Oxidation. *Adv. Funct. Mater.* **2024**, *34*, 2400806.
72. Ou, M.; Geng, M.; Fang, X.; Shao, W.; Bai, F.; Wan, S.; Ye, C.; Wu, Y.; Chen, Y. Tailored $BiVO_4$ photoanode hydrophobic microenvironment enables water oxidative H_2O_2 accumulation. *Adv. Sci.* **2023**, *10*, 2300169.
73. Wang, Q.; Ren, L.; Zhang, J.; Chen, X.; Chen, C.; Zhang, F.; Wang, S.; Wei, J. Recent Progress on the Catalysts and Device Designs for (Photo) Electrochemical On-Site H_2O_2 Production. *Adv. Energy Mater.* **2025**, *13*, 2301543.
74. Kim, J.H.; Hansora, D.; Sharma, P.; Jang, J.W.; Lee, J.S. Toward Practical Solar Hydrogen Production–An Artificial Photosynthetic Leaf-to-Farm Challenge. *Chem. Soc. Rev.* **2019**, *48*, 1908–1971.
75. Choi, H.; Seo, S.; Yoon, C.J.; Ahn, J.B.; Kim, C.S.; Jung, Y.; Kim, Y.; Toma, F.M.; Kim, H.; Lee, S. Organometal Halide Perovskite-Based Photoelectrochemical Module Systems for Scalable Unassisted Solar Water Splitting. *Adv. Sci.* **2023**, *10*, 2303106.
76. Hansora, D.; Yoo, J.W.; Mehrotra, R.; Byun, W.J.; Lim, D.; Kim, Y.K.; Noh, E.; Lim, H.; Jang, J.-W.; Seok, S.I.; et al. All-Perovskite-Based Unassisted Photoelectrochemical Water Splitting System for Efficient, Stable and Scalable Solar Hydrogen Production. *Nat. Energy* **2024**, *9*, 272–284.